Biomaterials 276 (2021) 121021

Contents lists available at ScienceDirect

Biomaterials

journal homepage: www.elsevier.com/locate/biomaterials

Magnetothermal regulation of in vivo protein corona formation on magnetic nanoparticles for improved cancer nanotherapy

Tingbin Zhang [a,1], Galong Li [b,1], Yuqing Miao [a], Junjie Lu [a], Ningqiang Gong [c], Yifan Zhang [a], Yuantai Sun [a], Yuan He [a], Mingli Peng [a], Xiaoli Liu [b], Xing-Jie Liang [c], Haiming Fan [a,b,*]

[a] Key Laboratory of Synthetic and Natural Functional Molecule of the Ministry of Education, College of Chemistry and Materials Science, Northwest University, Xi'an, 710069, China

[b] Key Laboratory of Resource Biology and Biotechnology in Western China, Ministry of Education, The College of Life Sciences & School of Medicine, Northwest University, Xi'an, 710069, China

[c] Laboratory of Controllable Nanopharmaceuticals, Chinese Academy of Sciences (CAS) Center for Excellence in Nanoscience and CAS Key Laboratory for Biomedical Effects of Nanomaterials and Nanosafety, National Center for Nanoscience and Technology, Beijing, 100190, China

ARTICLE INFO

Keywords:
Protein corona
In vivo magnetothermal regulation
Magnetic nanodrug
Pharmacokinetic behavior
Tumor delivery

ABSTRACT

Engineering the protein corona (PC) on nanodrugs is emerging as an effective approach to improve their pharmacokinetics and therapeutic efficacy, but conventional in vitro pre-programmed methods have shown great limitation for regulation of the PC in the complex and dynamic in vivo physiological environment. Here, we demonstrate an magnetothermal regulation approach that allows us to in situ modulate the in vivo PC composition on iron oxide nanoparticles for improved cancer nanotherapy. Experimental results revealed that the relative levels of major opsonins and dysopsonins in the PC can be tuned quantitatively by means of heat induction mediated by the nanoparticles under an alternating magnetic field. When the PC was magnetically optimized in vivo, the nanoparticles exhibited prolonged circulation and enhanced tumor delivery efficiency in mice, 2.53-fold and 2.02-fold higher respectively than the control. This led to a superior thermotherapeutic efficacy of systemically delivered nanoparticles. In vivo magnetothermal regulation of the PC on nanodrugs will find wide applications in biomedicine.

1. Introduction

Once nanoparticles contact complex biological fluids, their surfaces will rapidly adsorb proteins to form a coating termed the protein corona (PC) [1–3]. This "corona" layer is revealed to be tightly associated with the fate of nanoparticles in a rather unpredictable manner [4,5]. The PC is enriched in opsonins which increase the recognition and clearance of injected nanoparticles by the mononuclear phagocyte system (MPS). The MPS is the first and major barrier encountered by intravenously delivered nanodrugs, and results in majority of the injected dose loss after administration [6,7]. Therefore, an artificially engineered PC that can render the nanodrugs invisible to the MPS or even endow them with a specific targeting ability for enhanced therapeutic efficacy, has attracted much attention in recent years [8,9]. Various techniques based on pre-programmed nanoparticles, including tuning their size, shape and surface chemistry (i.e., ligand, charge, hydrophobicity), are being widely explored [10–13]. However, the corona formed in vivo by these methods is always inconsistent with that pre-designed in vitro [14,15]. Thus, the development of an in vivo corona regulation approach is highly desired to adapt to the complex and dynamic physiological environment.

Formation of the corona on nanoparticles is a complex process in which large numbers of proteins are simultaneously adsorbed via various noncovalent forces such as electrostatic, hydrogen bonding and hydrophobic interactions [16,17]. Proteins with high affinity for the nanoparticles ("hard" corona) are thought to be important in determining the biological identity of nanoparticles [18]. Accumulating evidence indicates that thermal energy can affect the adsorption kinetics of proteins onto nanoparticles [19,20]. An elevated incubation temperature is demonstrated to change the composition of the hard corona and

* Corresponding author. Key Laboratory of Synthetic and Natural Functional Molecule of the Ministry of Education, College of Chemistry and Materials Science, Northwest University, Xi'an, 710069, China.
E-mail address: fanhm@nwu.edu.cn (H. Fan).

[1] Tingbin Zhang and Galong Li contributed equally to this work.

https://doi.org/10.1016/j.biomaterials.2021.121021
Received 27 January 2021; Received in revised form 25 June 2021; Accepted 8 July 2021
Available online 10 July 2021

the degree of protein coverage on nanoparticles [21]. In particular, recent studies on gold nanorods revealed that localized heat induction generated by photon stimulation of the nanorods regulated their PC more efficiently than bulk heating did [22,23]. This shows the promising potential of in situ thermo-regulation of the PC. However, the limited penetration depth of photons and possible concerns about phototoxicity could hinder further in vivo application of this approach [24,25]. Magnetic nanoparticles are also attracting considerable interest because of their ability to mediate heat induction [26,27]. When an external alternating magnetic field (AMF) is applied, magnetic nanoparticles are "heated" due to hysteresis losses [28]. Magnetically induced heat has been widely applied for triggering biologically important events such as thermal activation of cellular ion channels for neuronal stimulation [29], thermal control of drug release [30] and remote modulation of enzyme activity for probing cellular function [31]. The AMF can penetrate the whole body, and therefore magnetic treatment appears to be a viable solution for in vivo regulation of the PC [32,33]. Moreover, biocompatible magnetic nanoparticles have been widely used as drug carriers, imaging agents, hyperthermia agents and iron supplements in preclinical and clinical settings [34,35]. In this context, the exploration of magnetothermal regulation of the in vivo PC formation on iron oxide nanoparticles (IONPs) is of particular interest for both biomedical research and clinical translation.

Here, we report the in vivo magnetothermal regulation of the PC on IONPs for the first time. Compared to the untreated IONPs, the AMF-treated IONPs formed a PC with reduced levels of opsonins and increased levels of dysopsonins, which is desirable for nanoparticles to escape from the MPS (Scheme 1). Experimental evidence revealed that both the PC composition and the pharmacokinetic behaviors of the IONPs were magnetic-field-dependent. In particular, IONPs with an in vivo magnetically modulated PC exhibited prolonged circulation time (2.53-fold longer) in normal mice and enhanced tumor accumulation (2.02-fold higher) in 4T1 tumor xenograft mice compared to untreated IONPs. Consequently, an augmented thermotherapeutic efficacy was observed for systematically delivered nanoparticles in the mouse tumor model. Our findings in this study open up the possibility of in vivo manipulation of the PC on nanodrugs for improved therapeutic efficacy.

2. Experimental section

2.1. Materials

1-Octadecene (99%), iron carboxylate (FeO(OH), 95%), oleic acid (90%), mouse serum albumin (>96%) and fluorescein isothiocyanate isomer I (FITC, 90%) were purchased from Sigma-Aldrich (MO, USA) and used as received. Phosphorylated poly (ethylene glycol)-methoxy (mPEG; M_w = 2000 Da) and phosphorylated PEG-NH_2 were supplied by Ruixi Biotech Co., Ltd. (Xi'an, China). Apo-B_{100} (>95%) was purchased from Otwo Biotech Co., Ltd. (Guangzhou, China). The BCA assay kit was supplied by Pierce (Rockford, IL). Lysotracker Deep Red was bought from Life Technologies (Molecular Probes, Eugene, OR). DAPI was purchased from Beijing Solarbio Science & Technology Co., Ltd. (Beijing, China). Ferumoxytol (Feraheme™) was bought from AMAG Pharmaceuticals (Waltham, MA).

2.2. Synthesis of IONPs

15 nm IONPs were synthesized by a previously developed thermal decomposition method [36]. The synthesis processes were as follows: 8 mmol of FeO(OH) and 40 mmol of oleic acid were dissolved in 20 g of 1-Octadecene. Under an argon gas atmosphere, the resulting brown solution was magnetically stirred for 30 min to remove H_2O. The temperature of the mixture was slowly heated to 180 °C and maintained for 1 h. Then the reaction temperature was heated to 320 °C under reflux for 1 h. The flask was cooled down to room temperature after the reaction. The black-brown solution was washed 2–3 times with hexane (10 mL) and acetone (20 mL), and centrifuged at 8000 rpm for 10 min. The hydrophobic Fe_3O_4 nanoparticles were dispersed in chloroform for the following experiments.

2.3. Preparation of phosphorylated mPEG-coated IONPs

The process of coating phosphorylated mPEG onto IONPs was carried out according to our previous work [37]. In a typical process, 50 mg of phosphorylated mPEG was added to the hydrophobic Fe_3O_4

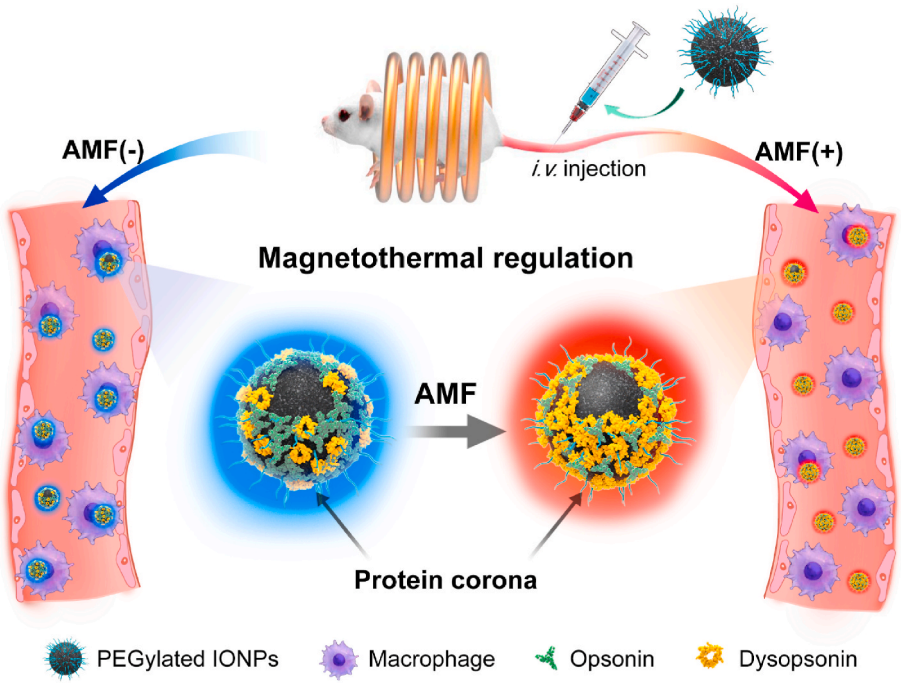

Scheme 1. Schematic illustration of in vivo magnetothermal regulation of the PC on IONPs. In-situ AMF exposure induces IONPs to generate localized heat and leads to changes in the opsonin and dysopsonin content of the PC, which further reduces sequestration by the MPS and alters the pharmacokinetic behavior of IONPs.

nanoparticles (10 mg) chloroform solution (10 mL), and sonicated for 10 min. The solution was continuously shaken for 5 h until the chloroform was completely evaporated. The dried nanoparticles were re-dispersed in deionized water, passed through a 0.22 μm syringe filter and dialyzed using 10 kDa cut-off dialysis bag to remove unbonded phosphorylated mPEG.

2.4. Characterization

X-ray powder diffraction pattern of IONPs was obtained on a Bruker D8 Advanced Diffractometer System equipped with Cu/Ka radiation in the 2θ range of 20–80°. The morphology and size of IONPs were examined by a FEI Talos F200X microscope operated at 200 KV. The magnetic properties of IONPs were characterized by a LakeShore Model 7407 Vibrating Sample Magnetometer (VSM) at room temperature. The hydrodynamic diameter and zeta potential of the IONPs were measured by a Zetasizer nano-ZS dynamic light scatting (DLS) instrument (Malvern, UK). The concentrations of Fe in each sample were determined using inductively coupled plasma mass spectrometry (ICP-MS). The concentrations of protein in each sample were determined by BCA assay. The proteins on IONPs were analyzed by 10% sodium dodecyl sulfate polyacrylamide gel electrophoresis (SDS-PAGE).

2.5. SAR measurements

To evaluate the inductive heating property of the IONPs, we tested their SAR under different alternating magnetic fields (AMFs) (f = 345 kHz, H = 200, 250 and 300 Oe) using a M5 induction heating system (Xi'an SuperMag Nano-biotechnology Co. Ltd, China). The concentration of IONPs was 0.2 mg Fe mL^{-1}. The temperature of the solution was detected using an optical fiber under the AMF in real time for 500 s. The formula for calculating the SAR value is as follows:

$$\mathrm{SAR} = C \frac{\Delta T}{\Delta t} \frac{1}{m_{\mathrm{Fe}}} \quad (1)$$

where C is the specific heat capacity of the solution, $\Delta T/\Delta t$ is the maximum slope of the heating inductive graph, and m_{Fe} is the weight fraction of Fe.

2.6. Protein corona formation

The whole blood was collected into heparinized (anticoagulant) tubes, and immediately centrifuged at 3000 rpm for 10 min at 4 °C to separate plasma from red and white blood cells [38]. 150 μL of IONPs (2.0 mg Fe mL^{-1}) was mixed with 1 mL of plasma, and incubated without or with AMF (f = 345 kHz, H = 200, 250 and 300 Oe) for 15 min. Then the mixtures were centrifuged at 15,000 g for 20 min at 4 °C, and the supernatant was removed. The nanoparticles were then resuspended in 1 mL of 10 mM PBS. This process was repeated three times to remove excess proteins and loosely-bound proteins. After the last centrifugation, only the proteins with high affinities (hard protein corona) remained. The hard protein corona was re-dispersed in SDT lysis buffer (4% SDS, 100 mM-Tris HCl and 1 mM DTT, pH 7.6), boiled for 5 min and sonicated for 2 min. The concentration of serum proteins in the supernatant was determined using the bicinchoninic assay (BCA) assay. For analysis of the in vivo PC components of IONPs (n = 3 mice), the blood samples were collected via the retro-orbital technique after 15 min of in vivo magnetothermal regulation. Plasma samples containing the PC-coated IONPs were obtained by centrifugation at 3000 rpm for 10 min at 4 °C. The subsequent procedure was the same as that for the in vitro samples.

2.7. LC-MS/MS

The obtained protein corona samples were further digested by filter-aided sample preparation (FASP digestion), desalted with a C18 Stage Tip and dried using a vacuum. Then the samples were redissolved in 0.1% formic acid in water for liquid chromatography coupled to mass spectrometry/mass spectrometry (LC-MS/MS) analysis. An appropriate amount of peptide was separated using a nanoliter flow rate Easy nLC 1200 chromatography system. Mobile phase A was 0.1% (v/v) formic acid in water, and mobile phase B was acetonitrile with 0.1% (v/v) formic acid (95% of acetonitrile). Afterwards, the peptides were separated and subjected to DDA (Data Dependent Acquisition) mass spectrometry using a Q-Exactive Plus mass spectrometer (Thermo Scientific). The analysis time was 60 min. The mass spectrometry data analysis and protein identification were used MaxQuant software (version 1.6.1.0) and Uniprot Mouse proteome database (http://www.uniprot.org/). The % of the total protein corona for each protein was determined using label-free quantification (LFQ) intensities relative to the total sum of protein LFQ intensities for each group. The cutoffs of global false discovery rate (FDR) $\leq$ 0.01 and Protein FDR $\leq$ 0.01 were used as screening criteria for peptide and protein identification, respectively.

2.8. Fluorescence quenching measurements

Alb and Apob were first labeled with FITC. Fluorescein isothiocyanate isomer I was dissolved in DMSO and slowly added to the protein solutions, with continuous stirring for 8 h at 4 °C. The unbound FITC was removed by repeated ultrafiltration with PBS. Quenching experiments were performed on a home-built optical-magnetic heat platform, which measured the fluorescence intensities of proteins with or without AMF in real time, while the solution temperature was measured using a thermal imager. The excitation wavelength was at 470 nm, and the emission spectra were collected from 490 to 700 nm. The concentrations of IONPs ranged from 0.1 to 2 nM, and the concentration of Alb-FITC or Apob-FITC was 1 μM.

In a typical process, the fluorescence quenching was dominated by diffusive transport when the concentrations of IONPs and proteins were extremely low. The results were fitted to the Stern-Volmer model, which is the standard model for analyzing fluorescence intensity data.

$$F_0 / F = 1 + K_q \tau_0 [\mathrm{IONPs}] = 1 + K_{sv} [\mathrm{IONPs}] \quad (2)$$

where F_0 and F are the maximum fluorescence intensities of the proteins in the absence and presence of IONPs, K_q is the quenching constant, τ_0 is the lifetime of the fluorophore (FITC), and [IONPs] is the concentration of quencher. K_{sv} is the Stern-Volmer quenching constant which is determined by the slope of the curves.

2.9. Internalization of nanoparticles into macrophages

RAW 264.7 macrophages were seeded in 6-well plates at 5 × 10^6 cells/well for 12 h. Then the medium was exchanged with serum-free DMEM for 1 h to starve the cells. The samples prepared to treat cells were as follows: (1) IONPs/PC formed by incubation with mouse plasma for 15 min, (2–4) IONPs/PC prepared by incubation with mouse plasma under AMF for 15 min (H = 200, 250 and 300 Oe, respectively). The obtained IONPs/PC were then added to cells at a concentration of 50 μg Fe mL^{-1} for 2 h at 37 °C. Next, the cells were washed three times with PBS and redispersed in 2 mL PBS. The cells were counted using a hemocytometer, then digested with 5 mL HNO_3 (MOS grade) and 2 mL H_2O_2 (MOS grade). Finally, the concentrations of Fe in the samples were determined using ICP-MS.

For confocal laser scanning microscopy (CLSM), phosphorylated mPEG (90%) and phosphorylated PEG-NH_2 (10%) were chosen to coat the surface of IONPs, and the NPs were further labeled by FITC. Lysosomes and nuclei were labeled by Lysotracker Deep Red and DAPI, respectively. RAW 264.7 cells were seeded in 35-mm glass dishes at 5 × 10^5 cells per dish and incubated overnight. The following procedures were the same as for the ICP-MS experiment. After the cells were stained

with Lysotracker Deep Red and DAPI, the samples were imaged by CLSM.

2.10. Pharmacokinetics

The pharmacokinetic profiles of IONPs with or without AMF exposure were examined in normal Balb/c mice (7–8 weeks old, about 24 g, n = 3). The mice administered with PBS were served as blank control group (background Fe). Before the administration of IONPs (5 mg Fe kg^{-1}), the mice were anesthetized with 1% pentobarbital sodium (40 mg per kg body weight) by intraperitoneal injection. For the group treated with AMF, the anesthetized mice were immediately exposed to AMF for 15 min after the administration of IONPs. At the designated time points (0.05, 0.167, 0.5, 1, 4, 8, 12 and 24 h), blood samples were collected into heparinized tubes by puncture of the retro-orbital sinus, then centrifuged at 3000 rpm for 10 min at 4 °C to obtain plasma. 10 μL plasma was predigested overnight at room temperature by adding 4 mL of concentrated nitric acid (HNO_3, MOS grade) and 1 mL of 30% hydrogen peroxide (H_2O_2, MOS grade) in sequence. Then the samples were further digested at 150 °C on a hot plate for 2 h. The remaining solution (about 0.5 mL) was diluted to 10 mL with 2% HNO_3. Finally, the concentrations of Fe in plasma were quantified using an Agilent 7900 ICP-MS (Agilent, Tokyo, Japan). % injected dose per mL plasma = (C_{Fe} × 1 mL)/(5 mg Fe kg^{-1} × W) × 100%, C_{Fe} stands for the concentration of Fe at each time point, W is the body weight of each mouse. The C_{Fe} for each sample have deducted the background Fe in plasma. Elimination half-life of the IONPs was calculated based on a two-compartment model using DAS 2.0 software. The procedure to analyze ferumoxytol pharmacokinetics was the same as for IONPs.

2.11. Biodistribution

The biodistribution of IONPs was studied in normal Balb/c mice (7–8 weeks old, about 24 g, n = 4). The mice were anesthetized through intraperitoneal injection of pentobarbital sodium (40 mg^{-1} kg, 1%) followed by i.v. administration of PBS or IONPs (5 mg Fe kg^{-1}). For the group treated with AMF, the anesthetized mice were immediately exposed to AMF for 15 min after the administration of IONPs. At the designated time-point (12 h), the mice were sacrificed and the major organs or tissues, including heart, liver, spleen, lung, kidney and brain, were excised, weighed and digested. Briefly, about 50 mg tissue samples were predigested overnight with 4 mL of HNO_3 and 1 mL 30% H_2O_2, then digested by heating for 2 h at 150 °C. When the solution volume was about 0.5 mL, the remaining solution was cooled and diluted to 50 mL with 2% HNO_3. Finally, the concentrations of Fe in each group were measured using ICP-MS. The procedure for determining the biodistribution of ferumoxytol was the same as for IONPs.

Besides, the distributions of IONPs in liver and spleen tissues were observed using DAB-enhanced Prussian Blue staining. The tissues were collected and fixed in 4% paraformaldehyde, paraffin-embedded and sectioned. The tissue sections were then stained with Prussian blue, DAB and hematoxylin dye, and at last observed with an optical microscope.

2.12. Cell culture and tumor xenograft model

4T1 and MCF-10A cells were cultured in complete RPMI 1640 medium containing 10% FBS and 1% antibiotic solution at 37 °C in 5% CO_2. The 4T1 xenograft tumor model (female, 6 weeks old) was generated by introducing a 4T1 cell suspension (1 × 10^6 cells) in PBS into the right flank of each Balb/c mouse. The animal experiment protocols were approved by the Animal Care and Use Committee of Northwest University, and complied with all relevant ethical regulations.

2.13. In vivo magnetic hyperthermia

The in vivo magnetic hyperthermia efficacy of IONPs was assessed in 4T1 xenograft tumor-bearing Balb/c mice. First, the tumor accumulation of IONPs with or without AMF (300 Oe) treatment was tested using the same procedure as for the biodistribution experiment. For the magnetic hyperthermia treatment (MHT) experiment, the tumor-bearing mice were randomly divided into 4 groups including PBS, IONPs/AMF, IONPs/MHT and IONPs/AMF/MHT (n = 4 mice per group). The mice were anesthetized through intraperitoneal injection of pentobarbital sodium (40 mg^{-1} kg, 1%) before i.v. injection of PBS or IONPs (5 mg Fe kg^{-1}). For the group treated with AMF, the anesthetized mice were immediately treated with AMF (300 Oe) for 15 min to modulate the protein corona. Magnetic hyperthermia was carried out by exposure to AMF (300 Oe) for 10 min at the indicated time points. The tumor size and body weight measurements were done by an investigator blinded to the treatments, and the tumor volumes were calculated according to $V = L \times W^2 \times 1/2$, where L and W represent the length and width of the tumor, respectively.

2.14. Statistical analysis

All experimental data are expressed as means ± SD, and $P < 0.05$ was regarded to be a statistically significant difference (*). Statistical analysis was performed using Graphpad prism 8.0 software. Two-tailed Student's t-test was used for comparisons between two groups. One-way analysis of variance (ANOVA) with Dunnett-t post hoc test was used to determine significant differences between multiple groups.

3. Results and discussion

3.1. In vitro magnetothermal regulation of the PC on IONPs

Monodisperse IONPs were prepared using a well-established thermal decomposition method [37]. To endow the obtained hydrophobic IONPs with good water dispersion, biocompatible phosphorylated PEG-methoxy (mPEG, M_w = 2000 Da) was chosen to modify their surface through the ligand exchange reaction. The X-ray diffraction (XRD) pattern of the as-prepared IONPs shows that all diffraction peaks matched well with the standard cubic spinel Fe_3O_4 power diffraction data (JCPDS no.19-0629) and no other impurities were found (Fig. S1A). TEM imaging revealed that the IONPs had a uniform spherical shape with an average diameter of ~13.1 nm (Fig. 1A). Decoration of the IONPs with phosphorylated mPEG was confirmed by Fourier transform infrared (FTIR) spectrum (Fig. S1B). The density of mPEG on IONPs was ~3.65 × 10^{-7} mol per mg, as determined by thermogravimetric (TG) analysis (Fig. S1C). The magnetic hysteresis loop of IONPs was characterized using a vibrating sample magnetometer (VSM). It showed a saturation magnetization (M_s) of 48.2 emu g^{-1} (Fig. S1D). No remanence or coercivity was observed, thus indicating the superparamagnetic nature of the obtained IONPs. Altogether, these results validated that the magnetic IONPs have been successfully prepared.

Then, we analyzed the PC that formed on the surface of the IONPs after in vitro incubation with mouse plasma. The IONPs were first incubated with plasma for 15 min, then separated from free proteins and the proteins with weak interactions (soft corona) by centrifugation at 15,000 g for 20 min [39], and finally washed three times to obtain PC-coated IONPs (IONPs/PC). The TEM image in Fig. 1A clearly shows a protein layer on the IONPs with an estimated thickness of 3 nm. The average hydrodynamic size of the IONPs changed from 33.0 to 42.4 nm after PC formation (Fig. 1B). SDS polyacrylamide gel electrophoresis (SDS-PAGE) showed that complex band patterns appeared and the majority of the bands were proteins with high molecular weights (>45 kDa) (Fig. S1E).

Further, we employed liquid chromatography coupled to mass spectrometry/mass spectrometry (LC-MS/MS) to investigate the capability of the magnetothermal regulation approach to manipulate the corona on IONPs (Fig. S2A). Since PC formation is a dynamic and rapid process [14], the AMF (frequency, f = 345 kHz; magnetic field

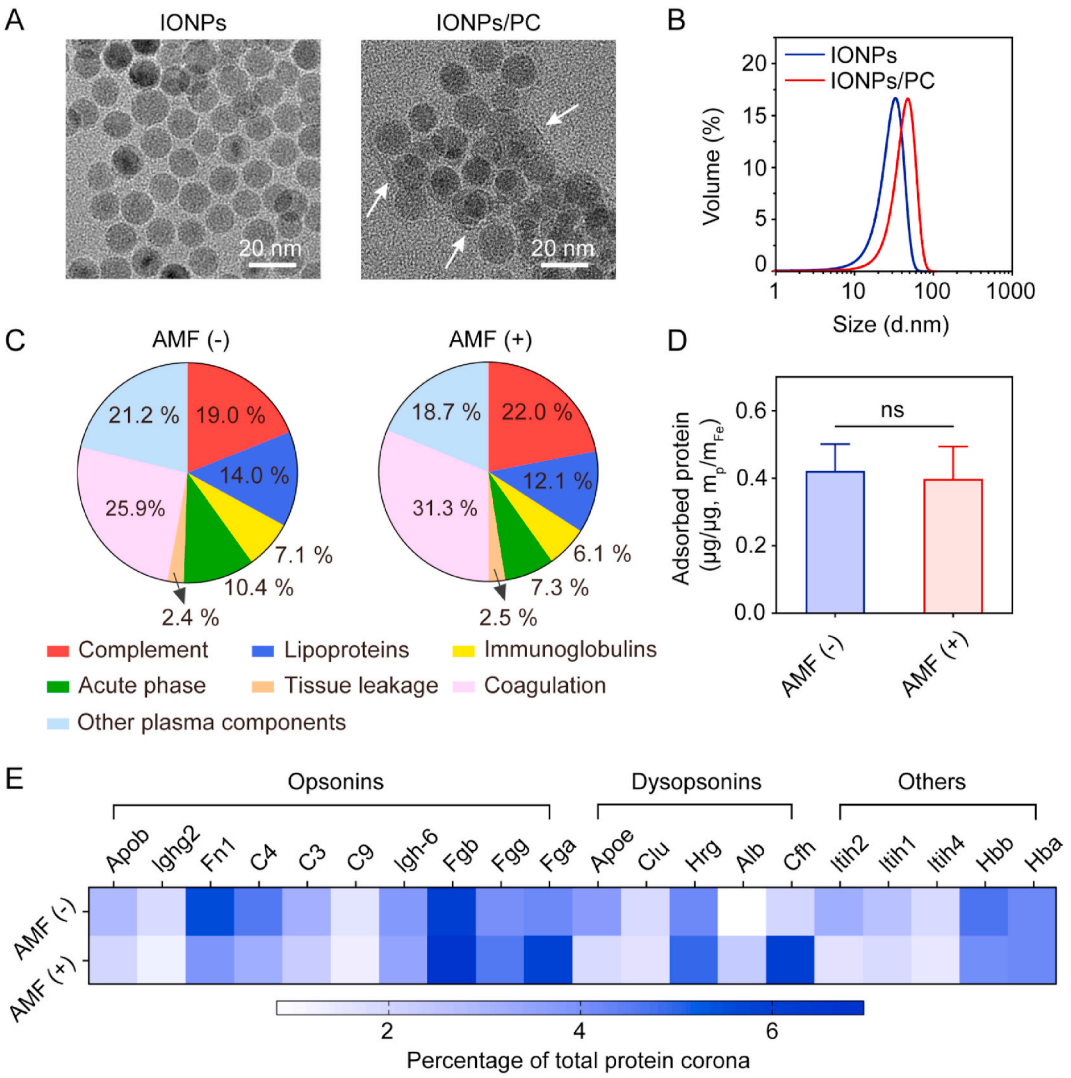

Fig. 1. Magnetothermal regulation of corona composition on IONPs in vitro. (A) TEM images of IONPs (left) and IONPs/PC (right). The PC was stained with 1% phosphotungstic acid. The white arrows in the IONPs/PC image indicate the PC on IONPs. Scale bar, 20 nm. (B) The hydrodynamic diameters of IONPs and IONPs/PC in aqueous solution. (C) Variation of corona components of IONPs with and without magnetothermal regulation determined by LC-MS/MS. The proteins in the corona were classified according to their biological functions. AMF conditions: $f = 345$ kHz and $H = 250$ Oe; duration, 15 min. (D) The amount of proteins adsorbed on IONPs with and without magnetothermal regulation determined by BCA assay. m_p, amount of protein; m_{Fe}, amount of Fe. ns = not significant ($P > 0.05$), analyzed by two-tailed Student's *t*-test. (E) Heat map showing the top 20 most abundant proteins (relative percentage > 1%) on IONPs with and without magnetothermal regulation identified by LC-MS/MS. The proteins were divided into three categories: opsonins, dysopsonins and others. Fga, Fgb and Fgg are three fibrinogen chains that form fibrinogen.

amplitude, $H = 250$ Oe) was applied upon addition of the IONPs into mouse plasma at room temperature and maintained for 15 min. When no AMF was applied, we identified 216 proteins in the PC, which can be classified into lipoproteins, immunoglobulins, complement proteins, coagulation factors, acute phase proteins, tissue leakage proteins and other proteins based on their biological functions (Fig. 1C). Upon magnetothermal regulation, the percentages of immunoglobulins, lipoproteins and acute phase proteins were reduced, and the percentages of complement proteins and proteins involved in coagulation were enhanced (Fig. 1C). This reveals the capability of this approach to manipulate the corona composition on IONPs. There is no significant difference in the gross amount of proteins bound on IONPs before and after magnetothermal regulation (Fig. 1D). It can be easily concluded that the magnetothermal regulation approach mainly changed the composition of the corona on IONPs rather than the amount of adsorbed proteins.

The differences in the top 20 most abundant proteins adsorbed on IONPs with or without magnetothermal regulation were summarized in a heat map (Fig. 1E and Table S1). The proteins were divided into three categories: opsonins, dysopsonins and others, according to whether the proteins promote or inhibit the phagocytosis of nanomaterials by macrophages [40]. The high content of opsonins, such as immunoglobulins and complement proteins, in the PC will raise the possibility of immunological recognition and macrophage capture of the nanoparticles, leading to a rapid clearance by the MPS [39,41]. In contrast, dysopsonins like serum albumin (Alb) and some apolipoproteins (such as clusterin, Clu) enable the nanoparticles to hide from the MPS and achieve a longer circulation time [42]. In total, eight opsonins were observed in the corona of untreated IONPs. Upon magnetothermal regulation, the percentages of seven opsonins were decreased, including a 31.7% decrease in apo-B_{100} (Apob) [43], and a 27.8% decrease in complement C3 (C3), a central component of the complement system [44]. Moreover, the percentages of complement factor H (Cfh) [45], a negative regulator of complement activation, and the dysopsonin Alb were enhanced 3.04-fold and 2.82-fold, respectively. According to early studies on the relationship between PC composition and MPS clearance

[18], these variations in the levels of corona components of IONPs after magnetothermal regulation are favorable for reducing their internalization by the MPS.

3.2. Mechanism behind magnetothermal regulation of the PC

We further investigated the mechanism underlying the magnetothermal regulation of the PC composition. First, the correlation between

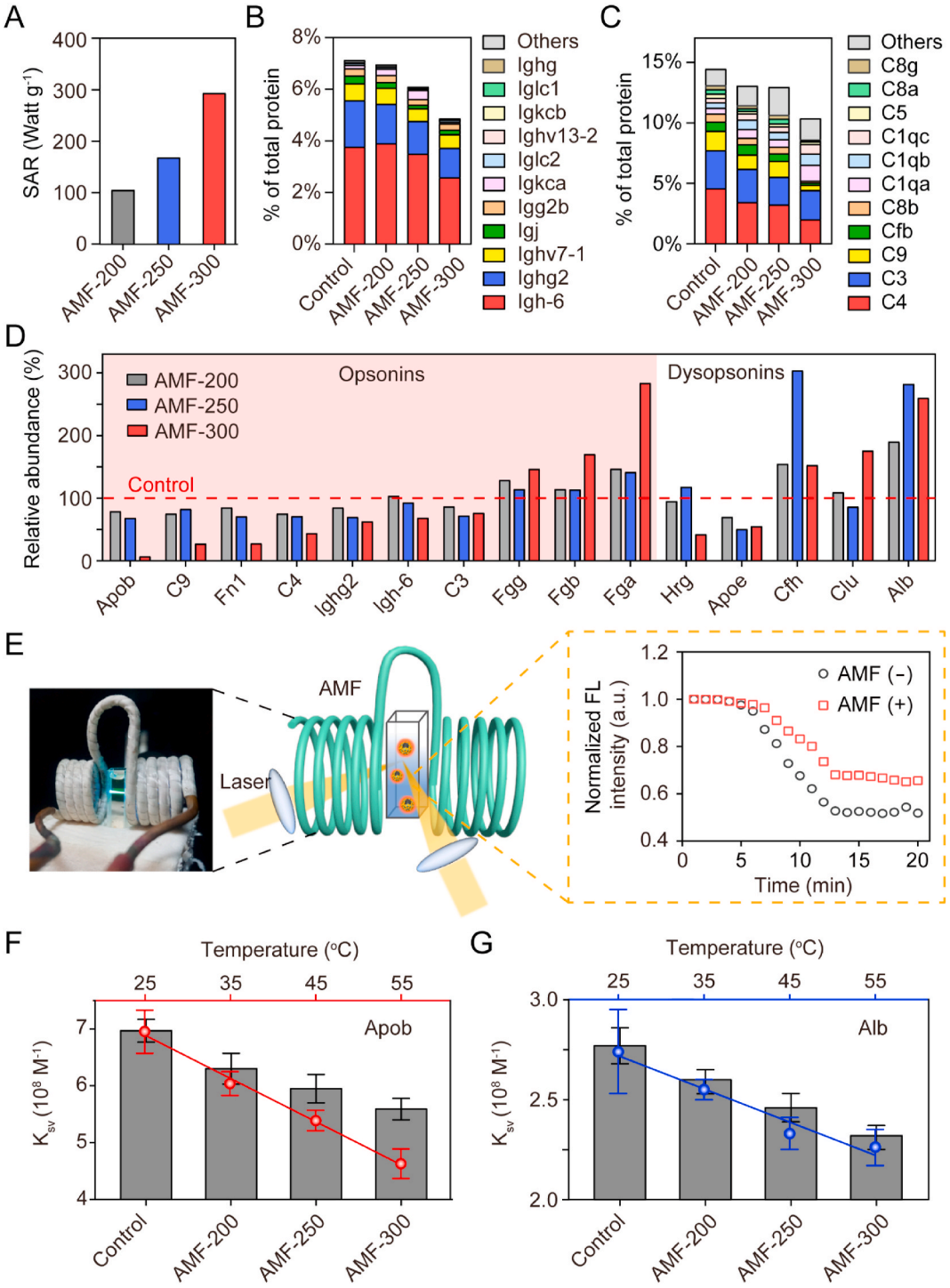

Fig. 2. Mechanism underlying magnetism-mediated corona regulation. (A) SAR values of IONPs with an iron concentration of 0.2 mg mL^{-1} under an AMF ($f = 345$ kHz; $H = 200$, 250 and 300 Oe). Variation of levels of immunoglobulins (B) and complement proteins (C) on IONPs with and without AMF treatment. The complement negative regulatory proteins are not included in (C) (for detailed information please see Fig. S2D). (D) The relative abundance of opsonins and dysopsonins in the top 20 PC components on IONPs with and without AMF treatment. The untreated IONPs served as control. (E) A home-built optical-magnetic heat platform to measure the fluorescence intensity of FITC-labeled proteins in real time under an AMF. The right panel is an example of the fluorescence intensity of Apob as a function of time in the presence and absence of AMF ($f = 345$ kHz; $H = 300$ Oe). The concentrations of Apob and IONPs were 1 μM and 1 nM, respectively. The K_{sv} values for Apob (F) and Alb (G) proteins after AMF treatment and water bath heating. Both Apob and Alb show a good linear correlation with water bath temperature (Apob, $R^2 = 0.99$; Alb, $R^2 = 0.95$).

AMF and corona composition was explored. Under the AMF, the IONPs can generate heat due to hysteresis losses, which is magnetic-field-dependent and increases with increasing *H*. For in vivo application, it is important to avoid potential side effects caused by magnetic hyperthermia during PC regulation. Therefore, we mimicked the in vivo environment (dosage: 66.7 μg Fe mL^{-1} equivalent to 5.0 mg Fe kg^{-1} per mouse, comparable to recent studies [46], solution: mouse plasma, temperature: 37 °C) and tested the heating of the sample after a 15 min AMF treatment (f = 345 kHz, H = 200–500 Oe) (Fig. S2B). When H exceeded 300 Oe, the sample temperature exceeded 41 °C, which is in the therapeutic temperature range (40–43 °C) of hyperthermia [47]. As a result, we chose an H for PC regulation ranging from 200 to 300 Oe in this study. The heat conversion efficiency of IONPs, i.e., the specific absorption rate (SAR), varied from 104.5 to 292.6 W g^{-1} (Fig. 2A and S2C). Upon magnetothermal regulation, we found that the percentages of immunoglobulins and complement proteins, which are common opsonins, were monotonously decreased with the increasing H, similar to the field dependence of SAR (Fig. 2B,C and S2D). Moreover, most opsonins in the top 20 PC components on IONPs were decreased with increasing H, while the dysopsonins were correspondingly increased (Fig. 2D and S2 D-I). Notably, opsonin Apob showed the biggest change, with a decrease of 92.8%. The dysopsonins Alb and Clu were greatly enhanced, by 2.60-fold and 1.76-fold respectively compared to the unmodulated PC (**Supplementary Document S1**). These results suggest that magnetothermal regulation of the corona on IONPs is magnetic-field-dependent, and may have a close relationship to the heat induction capability of IONPs, where a high H has a strong heating capability and induces more obvious variations of corona components.

Then, we investigated the influence of AMF on the interactions between IONPs and proteins using a fluorescence quenching assay. Apob and Alb as representatives of opsonins and dysopsonins in the PC on IONPs, were used as model proteins and labeled with FITC, while the IONP served as a quencher. Adsorption of FITC-labeled proteins on the surface of IONPs will quench the FITC fluorescence. As a result, the fluorescence intensity of FITC can reflect the binding affinity between IONPs and proteins [48]. To evaluate the binding properties of Apob and Alb to IONPs, the proteins were added dropwise into a solution of IONPs and the fluorescence intensities were measured in a real-time manner using a home-made optical measurement system consisting of a fluorescence spectrometer with an integrated AMF generator (Fig. 2E). The right panel in Fig. 2E shows the fluorescence intensity of Apob as a function of time in the presence of IONPs. Regardless of the presence or absence of AMF, the fluorescence intensity decreased initially due to adsorption of the protein onto IONPs and then stabilized after 13 min of incubation. A similar phenomenon was observed for the interaction between Alb and IONPs (Fig. S3), which suggests that 15 min of incubation is probably enough for the process of protein adsorption onto IONPs to reach an equilibrium state.

In the absence of AMF, the fluorescence intensities of Apob and Alb decreased with increasing concentrations of IONPs (Fig. S4A), which suggests a strong interaction between the proteins and the IONPs. For both Apob and Alb, the lowest fluorescence intensities were observed with no AMF, and relatively high fluorescence intensities were observed in the presence of AMF (Fig. S4A). This indicates that the binding affinity of these proteins to IONPs was reduced under AMF. The quenching data were fitted with the Stern-Volmer model, in which the slopes correspond to the quenching constant K_{sv} (Fig. S4B,C and Table S2). As shown in Fig. 2F and G, the K_{sv} values for both proteins are magnetic-field-dependent, with low K_{sv} values at high AMFs. A similar trend was also found when the proteins and IONPs were incubated with water bath heating (Fig. S5). The K_{sv} value decreased linearly as the water bath temperature increased (Fig. 2F and G). These results suggest that the induction heat under AMF should be responsible for the observed change in the adsorbed proteins on IONPs. In addition, because there was no obvious temperature rise during the whole 15 min AMF exposure owing to the very low Fe concentration (13.3 μg Fe mL^{-1}) (Fig. S6), the magnetic-field-dependent K_{sv} suggests that it is probably localized induction heat that modulated the protein-nanoparticle interactions, similar to the observation in magnetic induction heat-modulated enzyme activity [31]. Although it has been previously reported that physical stimuli such as light can change the PC composition [22], we are the first to discover that an AMF can quantitatively modulate the ratio of dysopsonins/opsonins in the PC of IONPs in a controllable manner. This finding is in contrast to the previous pre-programming methods, which always unpredictably change the percentages of opsonins or dysopsonins in the PC [10,14]. Moreover, the AMF-treated Apob or Alb in the presence of IONPs caused negligible toxicity effect in both MCF-10A and 4T1 cells (Fig. S7). Since AMF has no penetration limitation, the principle of PC magnetothermal regulation observed in vitro provides the unprecedented possibility for remote and real-time regulation of the PC of nanoparticles in vivo.

3.3. The impact of magnetothermal regulation on the in vivo fate of IONPs

Given the promising in vitro results, we further investigated the impact of magnetothermal regulation on the pharmacokinetic behaviors of IONPs in normal Balb/c mice (n = 3). The mice were anesthetized using pentobarbital sodium and administered with a dosage of 5 mg Fe kg^{-1} IONPs. For AMF-treated groups, the anesthetized mice were immediately transferred to the AMF coil for magnetothermal regulation (f = 345 kHz; H = 200, 250 and 300 Oe; t = 15 min) upon injection of IONPs. As shown in Fig. 3A and B, the untreated IONPs showed elimination half-life ($t_{1/2}$) of 5.33 h. In contrast, the AMF-treated groups showed prolonged $t_{1/2}$. Moreover, the in vivo circulation time of IONPs also showed a dependence on AMF, where increasing the AMF amplitude led to increased $t_{1/2}$ (Fig. 3B). The largest $t_{1/2}$ of 13.47 h was achieved for the group treated by the highest AMF (300 Oe) in this study (Table S3). Meanwhile, the treatment of IONPs/AMF caused negligible lysis of red blood cells (RBCs) at magnetic field amplitude as high as 300 Oe (Fig. S8), confirming that the high iron concentrations in blood of AMF-treated groups was not due to RBCs hemolysis. Furthermore, magnetothermal regulation of the non-magnetic mesoporous silica nanoparticles (MSNs) induced minimal effects on their pharmacokinetic behaviors (Fig. S9). This confirmed that the localized heat generated by IONPs under AMF should be responsible for the change in their pharmacokinetic behaviors. It is well known that most nanoparticles administered in vivo are sequestered by the MPS, resulting in rapid clearance and short circulation half-life [49,50]. These results clearly suggest that the AMF-treatment renders the ability of IONPs to evade MPS clearance. Recent studies revealed that the adsorption of opsonins on nanoparticles is mainly responsible for the MPS recognition and sequestration [51,52]. In accordance with in vitro results that magnetothermal regulation reduces the adsorption of opsonins on IONPs, we thus speculate that the prolonged $t_{1/2}$ of IONPs may be closely associated with the in-situ corona regulation by AMF. To verify this hypothesis, we first analyzed the PC composition of circulated IONPs with or without magnetothermal regulation. The PC-coated IONPs after the magnetothermal regulation were collected from blood samples, and the PC composition was analyzed by LC-MS/MS. Similar to the observation in vitro, the in vivo modulated PC also showed reduced level of opsonins and increased level of dysopsonins (Fig. 3C,D and S10 and Table S4). Specifically, the major opsonins such as C3 and C4 observed in vitro were also shown in vivo, while the predominant dysopsonins such as Alb and Clu observed in vitro were presented in vivo too (Supplementary Document S2). Moreover, the ratios of dysopsonins/opsonins in the PC modulated in vivo were monotonously increased from 51.2% to 76.7% with increasing H (Fig. 3D). These results suggested that our approach can also in vivo manipulate the levels of major opsonins and dysopsonins in the PC of IONPs. To test whether the modulated PC can indeed improve the $t_{1/2}$ of IONPs, we further examined the pharmacokinetic profile of IONPs that equipped with an in vitro magnetically modulated

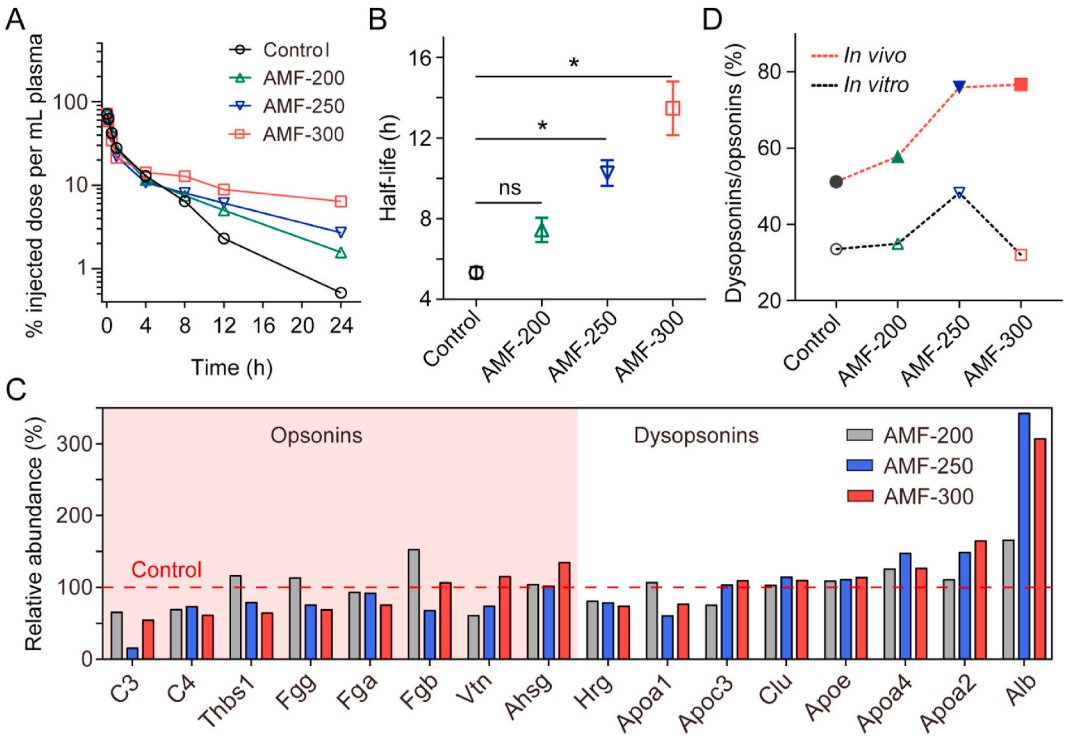

Fig. 3. The impact of in vivo magnetothermal regulation on the pharmacokinetic behaviors of IONPs. (A) Concentrations of IONPs in the bloodstream over time with or without AMF treatment. All data are fitted to a two-compartment pharmacokinetic model. n = 3 mice. (B) Elimination half-life of the IONPs with different treatments calculated with DAS 2.0 software. Mean values ± SD, n = 3. *$P < 0.05$, analyzed by one-way ANOVA with Dunnett-*t* adjustment. (C) The relative abundance of opsonins and dysopsonins in the top 20 PC components on injected IONPs with or without in vivo magnetothermal regulation. (D) Ratios of dysopsonins/opsonins in the top 20 PC components of IONPs after in vitro and in vivo magnetothermal regulation.

PC in normal Balb/c mice (n = 3). As expected, the IONPs with pre-modulated PC showed prolonged $t_{1/2}$ (1.88-fold increase) compared with the untreated IONPs (Fig. S11). Together, our results suggest that in vivo magnetic treatment can effectively manipulate the circulation half-life of IONPs via in situ PC regulation.

Since liver and spleen are the major MPS organs responsible for nanoparticles clearance [6], we further examined the biodistributions of AMF-treated IONPs in these tissues and compared with untreated IONPs in normal Balb/c mice (5 mg Fe kg^{-1}, n = 4). At the designated time-point (12 h) after i.v. injection, mice were sacrificed and the accumulation of IONPs in each organ was evaluated quantitatively using inductively coupled plasma-mass spectrometry (ICP-MS). In comparison with untreated IONPs, the AMF-treated groups exhibited decreased accumulation in liver and spleen, which showed a negative correlation with the AMF amplitude (Fig. 4A,B and S12). Notably, the accumulation of IONPs in the liver and spleen of mice exposed to an AMF of 300 Oe was decreased by 60.4% and 56.3% respectively, compared with mice receiving no AMF (Fig. 4A and B). Besides, we also isolated the liver and spleen tissues and visualized the IONPs using DAB-enhanced Prussian Blue staining. The lower accumulation in liver and spleen for AMF-treated groups were also observed in the images of DAB staining as compared with the untreated IONPs (Fig. 4C–F and S13–S15). These results prove that the AMF-treated IONPs can escape from MPS organs, which may result in prolonged circulation observed in the pharmacokinetic study. Moreover, we observed that the majority of IONPs accumulated in the sinusoid showed good colocalization with macrophages (Fig. 4C and S16). A similar phenomenon was also observed in spleen. The IONPs were mainly located in the red pulp zone, in which macrophages accumulated in a way similar to the hepatic sinusoid (Fig. 4E) [6]. These results indicated that the IONPs accumulated in liver and spleen are mainly captured by macrophages. It is well known that the PC composition of a nanoparticle can affect macrophage recognition and internalization [39]. We further investigated the effect of PC magnetothermal regulation on macrophage internalization of IONPs using a murine macrophage-like cell line (RAW 264.7). The IONPs/PC were prepared by incubating IONPs with mouse plasma under AMF for 15 min, and then added to the cells. Notably, RAW 264.7 cells incubated with IONPs/PC treated with an AMF of 300 Oe showed an obvious reduction (46.4%) in intracellular Fe content, and the uptake efficiency was negatively correlated with the *H* (Fig. S17A). Similar results were observed in fluorescence confocal images (Fig. S17B). Meanwhile, no obvious changes in the hydrodynamic sizes and zeta potentials were found for the IONPs before and after magnetothermal regulation (Fig. S17C and D). Taken together, our results provide the substantial evidence that the in situ corona regulation reduces the sequestration of IONPs by MPS, eventually leading to the prolonged circulation.

We further evaluated the biosafety and generality of the in vivo magnetothermal regulation approach in normal Balb/c mice (n = 3), which is critical for future clinical application. The mice receiving IONPs with a dosage of 5 mg Fe kg^{-1} and AMF at 300 Oe did not show any obvious changes in the major organs (heart, liver, spleen, lung, kidney and brain) (Fig. S18A). Further hematology and biochemistry assay results revealed that the levels of markers were comparable to those of mice from the PBS-treated group (Fig. S18B and C). These results demonstrate that magnetothermal regulation of the PC on IONPs is safe for in vivo applications. Notably, this approach does not involve any compounds or additional nanoparticles. This is in contrast to other MPS-blocking methods, such as administration of a high dose (>1 trillion) of nanoparticles or a low dose (1.25 mg kg^{-1}) of anti-erythrocyte antibodies to block MPS [53,54], where the excess nanoparticles or injected antibody may cause potential toxicity problems. We also tested the generality of our magnetothermal regulation approach using ferumoxytol, a clinically approved iron oxide nanoparticle used as an iron supplement [55]. Ferumoxytol has an iron core size of ~6.8 nm coated with polyglucose sorbitol carboxymethylether. The $t_{1/2}$ of untreated ferumoxytol (5 mg Fe kg^{-1} per mouse) in normal mice was 9.83 h, and the

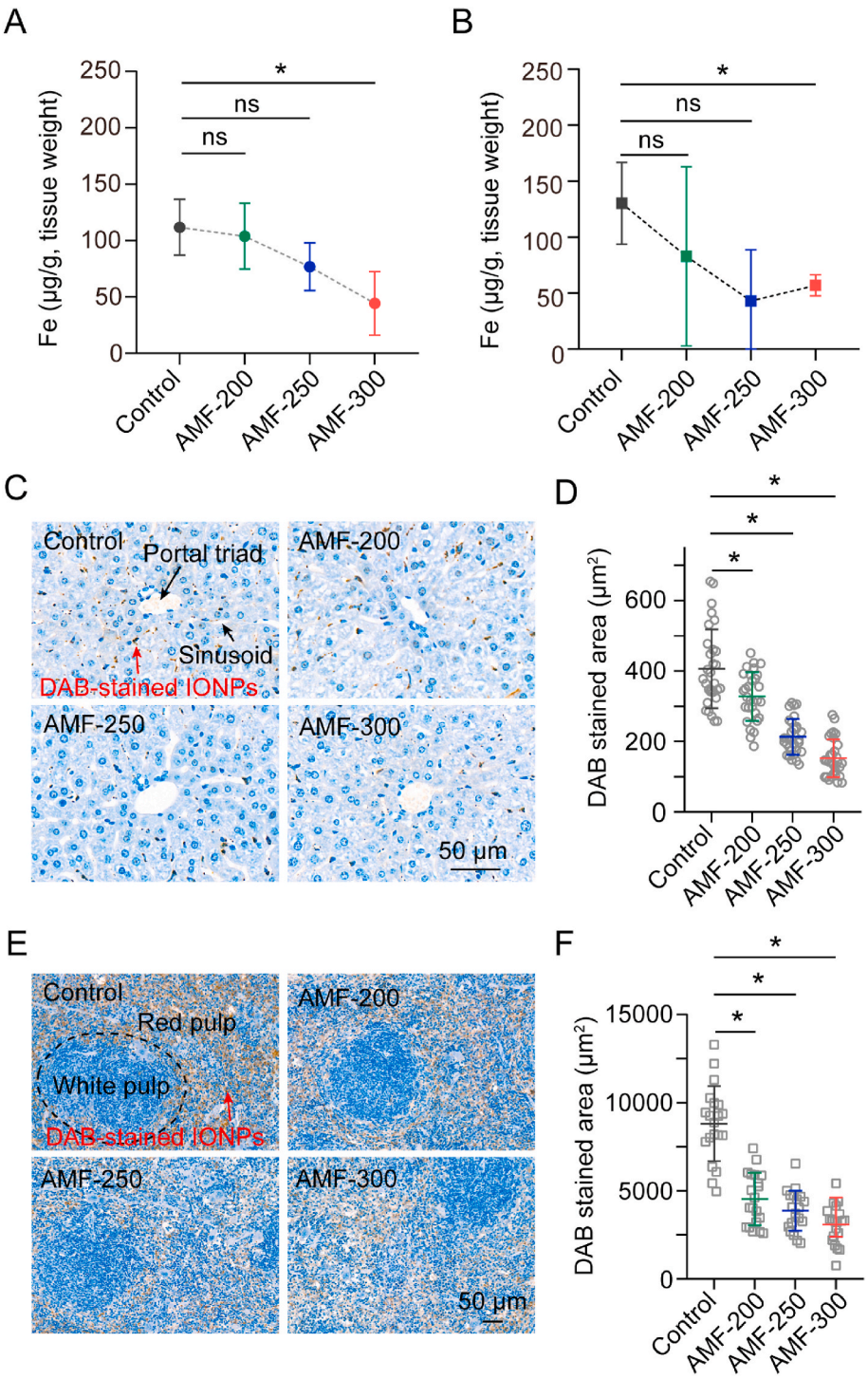

Fig. 4. The liver and spleen accumulation of AMF-treated IONPs in normal mice. Liver (A) and spleen (B) accumulation of IONPs 12 h post-injection as a function of AMF amplitude. The amount of Fe in liver was quantified using ICP-MS. The results shown in A and B have deducted the background Fe in liver and spleen. n = 3 mice. (C) DAB staining showing the distribution of IONPs in liver. Fe was stained with DAB (brown) and nuclei were stained with DAPI (blue). (D) Scatter plot showing the area of DAB staining in images of portal triad zone of liver with or without AMF treatment. Thirty images were analyzed for each group. (E) DAB staining showing the distribution of IONPs in spleen. (F) Scatter plot showing the area of DAB staining in images of spleen with or without AMF exposure. Twenty images were analyzed for each group. Scale bar, 50 μm. Mean values ± SD. ns = not significant ($P > 0.05$); *$P < 0.05$, analyzed by one-way ANOVA with Dunnett-*t* adjustment. (For interpretation of the references to colour in this figure legend, the reader is referred to the Web version of this article.)

majority of injected nanoparticles accumulated in the liver and spleen (Fig. S19 and Table S5). Upon magnetothermal regulation ($f = 345$ kHz; $H = 300$ Oe), we observed that liver and spleen accumulation of the injected nanoparticles was decreased, and the $t_{1/2}$ was increased to 25.45 h. These results suggest that magnetothermal regulation is a universal PC-modulating approach regardless of the size and surface chemistry of IONPs. Since AMF has been approved for clinical treatment of glioblastoma [56], the magnetothermal regulation approach can be immediately applied in clinical settings to improve the pharmacokinetics of magnetic nanodrugs.

3.4. *In vivo cancer therapeutic application*

To exploit the potential utility of our PC magnetothermal regulation approach in cancer medicine, we explored the impact of in vivo magnetothermal regulation on the IONPs-based systematically delivered nanothermotherapy. Magnetic hyperthermia treatment (MHT) using IONPs is a clinically approved modality for cancer therapy [56]. However, the systemic delivery of therapeutic heat has been a challenge due to insufficient tumor accumulation of IONPs nanoheaters [57]. Increasingly evidences showed that the prolonged circulation can enhance the chance for nanoparticles to accumulate in the tumor [58],

which might consequently improve the efficacy of systemically delivered MHT. We thus evaluated the efficacy of systemically delivered MHT using magnetically modulated IONPs in a subcutaneous 4T1 murine breast cancer model. Fig. 5A shows a schematic depiction of the treatment schedule. When the tumor volume reached approximately 100 mm^3, the IONPs were intravenously administered at a dose of 5 mg Fe kg^{-1} per mouse (female, 6 weeks old, n = 4). The mice were anesthetized using pentobarbital sodium and exposed to AMF at 300 Oe for 15 min immediately upon injection for PC regulation. MHT was then carried out for 10 min at the designated time points. We first studied the effect of magnetothermal regulation on the biodistribution (12 h) of IONPs in tumor-bearing mice (n = 3). As shown in Fig. 5B, both the liver and spleen accumulation of AMF-treated IONPs were decreased in comparison with untreated IONPs, which are similar to our previous observations in normal mice. However, the tumor accumulation of AMF-treated IONPs showed an obvious enhancement, 2.02-fold larger than that of untreated IONPs (Fig. 5B and S20). As a result, the tumor inhibition efficacy in the IONPs/AMF/MHT group (65.4% inhibition) was much higher than in the IONPs/AMF group (9.1%) and the IONPs/MHT group (26.6%) (Fig. 5C). The superior therapeutic outcome of the IONPs/AMF/MHT group was further verified by collecting and weighing the tumors from the different groups (Fig. 5D and S21). In addition, no significant decrease in mouse body weight was observed during the whole experimental period (Fig. 5E). Our results demonstrated that in vivo magnetothermal regulation can indeed improve the tumor accumulation of IONPs and MHT efficacy in tumor-bearing mice. As IONPs have been widely used in cancer diagnosis and treatment such as the contrast agents for magnetic resonance imaging [59], and the carriers for chemotherapy or immunotherapy [60], the markedly improved MHT efficacy demonstrates the potential of our magnetothermal regulation approach for enhancing the accuracy of tumor diagnosis, and the effectiveness of chemotherapy or immunotherapy for tumor treatment.

4. Conclusion

In summary, we have developed a magnetothermal regulation approach that allows us to quantitatively manipulate the in vivo PC composition of iron oxide based magnetic nanodrugs. This magnetothermal regulation technique utilizes localized induction heat generated by IONPs under AMF to modulate the PC composition during the formation process. Both in vitro and in vivo results showed that the magnetothermal regulation led to the modulated PC with down-regulated opsonins and up-regulated dysopsonins. Beneficial from the PC regulation, AMF-treated IONPs showed improved pharmacokinetic behaviors including prolonged blood circulation (2.53-fold increase) and reduced liver (60.4% decrease) and spleen (56.3% decrease) accumulation, which eventually led to superior efficacy of cancer nanotherapy. Our approach also succeeded in improving the in vivo behaviors of the clinically available IONP nanodrug ferumoxytol, showing great potential in clinic application. Ultimately, this work demonstrates a universal magnetic approach for regulation of the in vivo corona composition on magnetic nanoparticles, which thus opens up the new possibility of in situ altering the in vivo fate of nanodrugs towards efficient cancer nanotherapy.

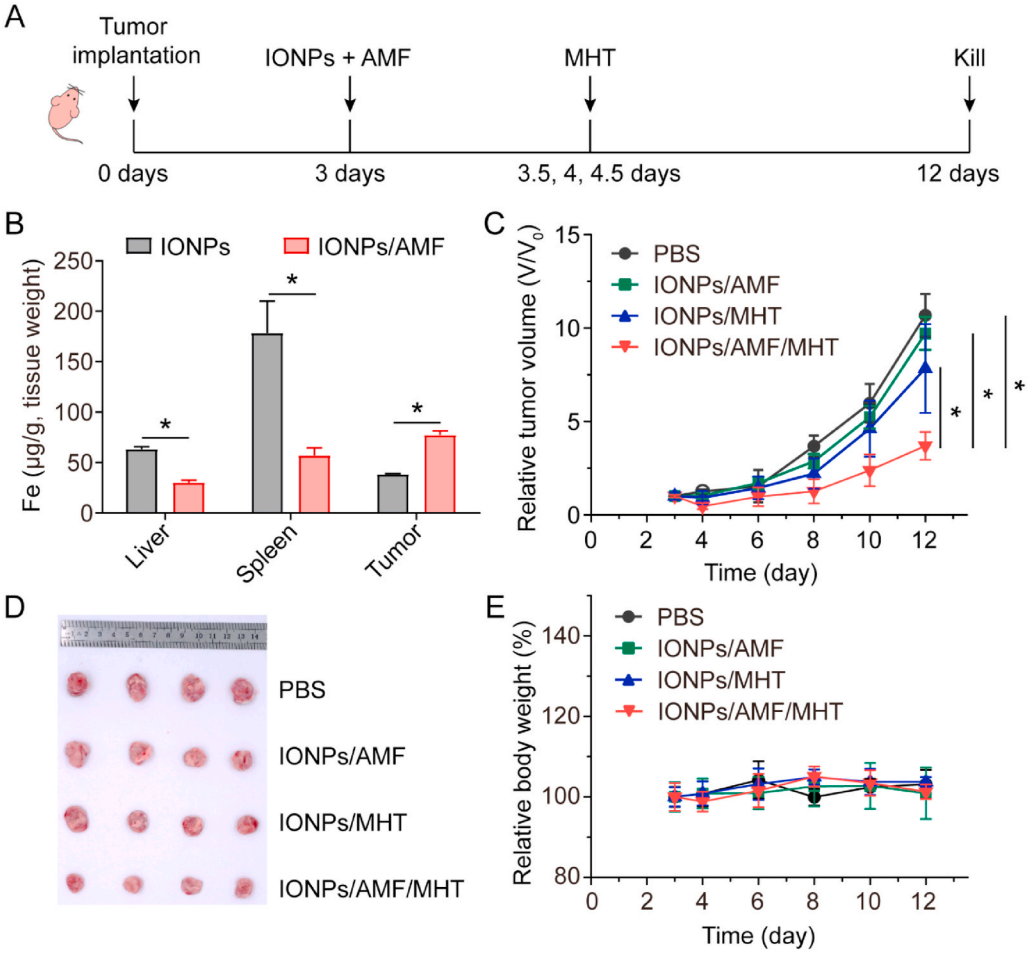

Fig. 5. In vivo magnetic hyperthermia assessment. (A) Scheme of the magnetic hyperthermia treatment schedule in a 4T1 xenograft tumor model. For magnetothermal regulation, anesthetized mice were exposed to AMF for 15 min at 300 Oe. For MHT, anesthetized mice were exposed to AMF for 10 min at 300 Oe at the indicated time points. (B) Comparison of the liver, spleen and tumor accumulation of IONPs with and without exposure to AMF. The content of Fe in these tissues was analyzed 12 h after i.v. injection (5 mg Fe kg^{-1} per mouse, n = 3). The results shown in B have deducted the background Fe in tissues. Mean values ± SD. *$P < 0.05$, analyzed by two-tailed Student's *t*-test. (C) Plot of tumor volume (V/V_0) versus time after treatment with different groups (5 mg Fe kg^{-1} per mouse, n = 4). Mean values ± SD. *$P < 0.05$, analyzed by one-way ANOVA with Dunnett-*t* adjustment. (D) Digital photos of tumor tissues harvested from mice at the end of treatment. (E) Graph showing mouse relative body weights in the different groups during the experimental period.

Declaration of competing interest

The authors declare that they have no known competing financial interests or personal relationships that could have appeared to influence the work reported in this paper.

Acknowledgements

This work was financially supported by the National Natural Science Foundation of China (NSFC) (grant numbers 32001005, 81771981, 82072063, 22072115 and 31901003), the NSFC international collaboration key project (grant number 51861135103), the Shaanxi Province Funds for Distinguished Young Scholars (grant number 202031900097), the Natural Science Foundation of Shaanxi Province (grant numbers 2020JQ610, 2021JQ-438 and 2019JM143) and the Postdoctoral Science Foundation of China (grant number 2020M673631XB). We thank Huijun Ma from the National Demonstration Center for Experimental Chemistry Education of Northwest University for the TEM characterization.

Appendix A. Supplementary data

Supplementary data to this article can be found online at https://doi.org/10.1016/j.biomaterials.2021.121021.

Data availability

The raw/processed data required to reproduce these findings cannot be shared at this time as the data also forms part of an ongoing study.

Credit author statement

Tingbin Zhang: Investigation, Data curation, Formal analysis, Methodology, Resources, Writing – original draft, Writing – review & editing, Funding acquisition. Galong Li: Investigation, Data curation, Formal analysis, Visualization, Writing – review & editing, Funding acquisition. Yuqing Miao: Investigation, Resources, Visualization. Junjie Lu: Investigation, Methodology. Ningqiang Gong: Investigation, Resources, Writing – review & editing. Yifan Zhang: Investigation, Validation. Yuantai Sun: Investigation. Yuan He: Writing – review & editing. Mingli Peng: Writing – review & editing, Funding acquisition. Xiaoli Liu: Formal analysis, Resources, Validation. Xing-Jie Liang: Resources, Writing – review & editing, Funding acquisition. Haiming Fan: Conceptualization, Supervision, Resources, Project administration, Writing – review & editing, Funding acquisition.

References

[1] T. Cedervall, I. Lynch, S. Lindman, T. Berggard, E. Thulin, H. Nilsson, K.A. Dawson, S. Linse, Understanding the nanoparticle-protein corona using methods to quantify exchange rates and affinities of proteins for nanoparticles, Proc. Natl. Acad. Sci. U. S.A. 104 (2007) 2050–2055.
[2] A. Salvati, A.S. Pitek, M.P. Monopoli, K. Prapainop, F.B. Bombelli, D.R. Hristov, P. M. Kelly, C. Aberg, E. Mahon, K.A. Dawson, Transferrin-functionalized nanoparticles lose their targeting capabilities when a biomolecule corona adsorbs on the surface, Nat. Nanotechnol. 8 (2013) 137–143.
[3] M.M. Yallapu, N. Chauhan, S.F. Othman, V. Khalilzad-Sharghi, M.C. Ebeling, S. Khan, M. Jaggi, S.C. Chauhan, Implications of protein corona on physico-chemical and biological properties of magnetic nanoparticles, Biomaterials 46 (2015) 1–12.
[4] M. Hadjidemetriou, K. Kostarelos, Nanomedicine: evolution of the nanoparticle corona, Nat. Nanotechnol. 12 (2017) 288–290.
[5] A.K. Barui, J.Y. Oh, B. Jana, C. Kim, J.-H. Ryu, Cancer-targeted nanomedicine: overcoming the barrier of the protein corona, Adv. Ther. 3 (2020) 1900124.
[6] S. Wilhelm, A.J. Tavares, Q. Dai, S. Ohta, J. Audet, H.F. Dvorak, W.C.W. Chan, Analysis of nanoparticle delivery to tumours, Nat. Rev. Mater. 1 (2016) 16014.
[7] P. Sánchez-Moreno, P. Buzón, H. Boulaiz, J.M. Peula-García, J.L. Ortega-Vinuesa, I. Luque, A. Salvati, J.A. Marchal, Balancing the effect of corona on therapeutic efficacy and macrophage uptake of lipid nanocapsules, Biomaterials 61 (2015) 266–278.
[8] P.C. Ke, S. Lin, W.J. Parak, T.P. Davis, F. Caruso, A decade of the protein corona, ACS Nano 11 (2017) 11773–11776.
[9] Z. Zhang, J. Guan, Z. Jiang, Y. Yang, J. Liu, W. Hua, Y. Mao, C. Li, W. Lu, J. Qian, C. Zhan, Brain-targeted drug delivery by manipulating protein corona functions, Nat. Commun. 10 (2019) 3561.
[10] M. Lundqvist, J. Stigler, G. Elia, I. Lynch, T. Cedervall, K.A. Dawson, Nanoparticle size and surface properties determine the protein corona with possible implications for biological impacts, Proc. Natl. Acad. Sci. U.S.A. 105 (2008) 14265–14270.
[11] R. García-Álvarez, M. Hadjidemetriou, A. Sánchez-Iglesias, L.M. Liz-Marzán, K. Kostarelos, In vivo formation of protein corona on gold nanoparticles. The effect of their size and shape, Nanoscale 10 (2018) 1256–1264.
[12] Z. Li, Y. Wang, J. Zhu, Y. Zhang, W. Zhang, M. Zhou, C. Luo, Z. Li, B. Cai, S. Gui, Z. He, J. Sun, Emerging well-tailored nanoparticulate delivery system based on in situ regulation of the protein corona, J. Contr. Release 320 (2020) 1–18.
[13] J. Müller, K.N. Bauer, D. Prozeller, J. Simon, V. Mailänder, F.R. Wurm, S. Winzen, K. Landfester, Coating nanoparticles with tunable surfactants facilitates control over the protein corona, Biomaterials 115 (2017) 1–8.
[14] S. Tenzer, D. Docter, J. Kuharev, A. Musyanovych, V. Fetz, R. Hecht, F. Schlenk, D. Fischer, K. Kiouptsi, C. Reinhardt, K. Landfester, H. Schild, M. Maskos, S. K. Knauer, R.H. Stauber, Rapid formation of plasma protein corona critically affects nanoparticle pathophysiology, Nat. Nanotechnol. 8 (2013) 772–781.
[15] X. Lu, P. Xu, H.-M. Ding, Y.-S. Yu, D. Huo, Y.-Q. Ma, Tailoring the component of protein corona via simple chemistry, Nat. Commun. 10 (2019) 4520.
[16] O. Vilanova, J.J. Mittag, P.M. Kelly, S. Milani, K.A. Dawson, J.O. Rädler, G. Franzese, Understanding the kinetics of protein–nanoparticle corona formation, ACS Nano 10 (2016) 10842–10850.
[17] M. De, C.-C. You, S. Srivastava, V.M. Rotello, Biomimetic interactions of proteins with functionalized nanoparticles: A thermodynamic study, J. Am. Chem. Soc. 129 (2007) 10747–10753.
[18] Walkey Carl, Chan Warren, Understanding and controlling the interaction of nanomaterials with proteins in a physiological environment, Chem. Soc. Rev. 41 (2012) 2780–2799.
[19] M. Mahmoudi, I. Lynch, M.R. Ejtehadi, M.P. Monopoli, F.B. Bombelli, S. Laurent, Protein−nanoparticle interactions: opportunities and challenges, Chem. Rev. 111 (2011) 5610–5637.
[20] M. Mahmoudi, M.A. Shokrgozar, S. Behzadi, Slight temperature changes affect protein affinity and cellular uptake/toxicity of nanoparticles, Nanoscale 5 (2013) 3240–3244.
[21] M. Mahmoudi, A.M. Abdelmonem, S. Behzadi, J.H. Clement, S. Dutz, M. R. Ejtehadi, R. Hartmann, K. Kantner, U. Linne, P. Maffre, S. Metzler, M. K. Moghadam, C. Pfeiffer, M. Rezaei, P. Ruiz-Lozano, V. Serpooshan, M. A. Shokrgozar, G.U. Nienhaus, W.J. Parak, Temperature: the "ignored" factor at the nanobio interface, ACS Nano 7 (2013) 6555–6562.
[22] M. Mahmoudi, S.E. Lohse, C.J. Murphy, A. Fathizadeh, A. Montazeri, K.S. Suslick, Variation of protein corona composition of gold nanoparticles following plasmonic heating, Nano Lett. 14 (2014) 6–12.
[23] E. Polo, V. Araban, B. Pelaz, A. Alvarez, P. Taboada, M. Mahmoudi, P. del Pino, Photothermal effects on protein adsorption dynamics of PEGylated gold nanorods, Appl. Mater. Today 15 (2019) 599–604.
[24] R.A. Hoebe, C.H. Van Oven, T.W.J. Gadella, P.B. Dhonukshe, C.J.F. Van Noorden, E.M.M. Manders, Controlled light-exposure microscopy reduces photobleaching and phototoxicity in fluorescence live-cell imaging, Nat. Biotechnol. 25 (2007) 249–253.
[25] S. Mura, J. Nicolas, P. Couvreur, Stimuli-responsive nanocarriers for drug delivery, Nat. Mater. 12 (2013) 991–1003.
[26] G. Song, M. Kenney, Y.-S. Chen, X. Zheng, Y. Deng, Z. Chen, S.X. Wang, S. S. Gambhir, H. Dai, J. Rao, Carbon-coated FeCo nanoparticles as sensitive magnetic-particle-imaging tracers with photothermal and magnetothermal properties, Nat. Biomed. Eng. 4 (2020) 325–334.
[27] N.A. Stocke, P. Sethi, A. Jyoti, R. Chan, S.M. Arnold, J.Z. Hilt, M. Upreti, Toxicity evaluation of magnetic hyperthermia induced by remote actuation of magnetic nanoparticles in 3D micrometastasic tumor tissue analogs for triple negative breast cancer, Biomaterials 120 (2017) 115–125.
[28] V.F. Cardoso, A. Francesko, C. Ribeiro, M. Bañobre-López, P. Martins, S. Lanceros-Mendez, Advances in magnetic nanoparticles for biomedical applications, Adv. Healthcare Mater. 7 (2018) 1700845.
[29] D. Rosenfeld, A.W. Senko, J. Moon, I. Yick, P. Anikeeva, Transgene-free remote magnetothermal regulation of adrenal hormones, Sci. Adv. 6 (2020) eaaz3734.
[30] A.M. Derfus, G. von Maltzahn, T.J. Harris, T. Duza, K.S. Vecchio, E. Ruoslahti, S. N. Bhatia, Remotely triggered release from magnetic nanoparticles, Adv. Mater. 19 (2007) 3932–3936.
[31] R. Xiong, W. Zhang, Y. Zhang, Y. Zhang, Y. Chen, Y. He, H. Fan, Remote and real time control of an FVIO–enzyme hybrid nanocatalyst using magnetic stimulation, Nanoscale 11 (2019) 18081–18089.
[32] N. Lee, D. Yoo, D. Ling, M.H. Cho, T. Hyeon, J. Cheon, Iron oxide based nanoparticles for multimodal imaging and magnetoresponsive therapy, Chem. Rev. 115 (2015) 10637–10689.
[33] X. Liu, J. Zheng, W. Sun, X. Zhao, Y. Li, N. Gong, Y. Wang, X. Ma, T. Zhang, L.-Y. Zhao, Y. Hou, Z. Wu, Y. Du, H. Fan, J. Tian, X.-J. Liang, Ferrimagnetic vortex nanoring-mediated mild magnetic hyperthermia imparts potent immunological effect for treating cancer metastasis, ACS Nano 13 (2019) 8811–8825.
[34] S. Zanganeh, G. Hutter, R. Spitler, O. Lenkov, M. Mahmoudi, A. Shaw, J. S. Pajarinen, H. Nejadnik, S. Goodman, M. Moseley, Iron oxide nanoparticles inhibit tumour growth by inducing pro-inflammatory macrophage polarization in tumour tissues, Nat. Nanotechnol. 11 (2016) 986–994.

[35] M. Colombo, S. Carregal-Romero, M.F. Casula, L. Gutiérrez, M.P. Morales, I. B. Böhm, J.T. Heverhagen, D. Prosperi, W.J. Parak, Biological applications of magnetic nanoparticles, Chem. Soc. Rev. 41 (2012) 4306–4334.
[36] J. Park, K. An, Y. Hwang, J.-G. Park, H.-J. Noh, J.-Y. Kim, J.-H. Park, N.-M. Hwang, T. Hyeon, Ultra-large-scale syntheses of monodisperse nanocrystals, Nat. Mater. 3 (2004) 891–895.
[37] X.L. Liu, H.M. Fan, J.B. Yi, Y. Yang, E.S.G. Choo, J.M. Xue, D.D. Fan, J. Ding, Optimization of surface coating on Fe_3O_4 nanoparticles for high performance magnetic hyperthermia agents, J. Mater. Chem. 22 (2012) 8235–8244.
[38] S. Schöttler, G. Becker, S. Winzen, T. Steinbach, K. Mohr, K. Landfester, V. Mailänder, F.R. Wurm, Protein adsorption is required for stealth effect of poly (ethylene glycol)- and poly(phosphoester)-coated nanocarriers, Nat. Nanotechnol. 11 (2016) 372–377.
[39] K. Saha, M. Rahimi, M. Yazdani, S.T. Kim, D.F. Moyano, S. Hou, R. Das, R. Mout, F. Rezaee, M. Mahmoudi, V.M. Rotello, Regulation of macrophage recognition through the interplay of nanoparticle surface functionality and protein corona, ACS Nano 10 (2016) 4421–4430.
[40] R. Cai, C. Chen, The crown and the scepter: roles of the protein corona in nanomedicine, Adv. Mater. 31 (2019) 1805740.
[41] S. Ritz, S. Schöttler, N. Kotman, G. Baier, A. Musyanovych, J. Kuharev, K. Landfester, H. Schild, O. Jahn, S. Tenzer, V. Mailänder, Protein corona of nanoparticles: distinct proteins regulate the cellular uptake, Biomacromolecules 16 (2015) 1311–1321.
[42] Q. Dai, N. Bertleff-Zieschang, J.A. Braunger, M. Björnmalm, C. Cortez-Jugo, F. Caruso, Particle targeting in complex biological media, Adv. Healthcare Mater. 7 (2018) 1700575.
[43] S. Lara, F. Alnasser, E. Polo, D. Garry, M.C. Lo Giudice, D.R. Hristov, L. Rocks, A. Salvati, Y. Yan, K.A. Dawson, Identification of receptor binding to the biomolecular corona of nanoparticles, ACS Nano 11 (2017) 1884–1893.
[44] T. Fujita, Evolution of the lectin–complement pathway and its role in innate immunity, Nat. Rev. Immunol. 2 (2002) 346–353.
[45] K. Yu, B.F.L. Lai, J.H. Foley, M.J. Krisinger, E.M. Conway, J.N. Kizhakkedathu, Modulation of complement activation and amplification on nanoparticle surfaces by glycopolymer conformation and chemistry, ACS Nano 8 (2014) 7687–7703.
[46] H.A. Albarqi, L.H. Wong, C. Schumann, F.Y. Sabei, T. Korzun, X. Li, M.N. Hansen, P. Dhagat, A.S. Moses, O. Taratula, O. Taratula, Biocompatible nanoclusters with high heating efficiency for systemically delivered magnetic hyperthermia, ACS Nano 13 (2019) 6383–6395.
[47] P. Wust, B. Hildebrandt, G. Sreenivasa, B. Rau, J. Gellermann, H. Riess, R. Felix, P. M. Schlag, Hyperthermia in combined treatment of cancer, Lancet Oncol. 3 (2002) 487–497.
[48] S.P. Boulos, T.A. Davis, J.A. Yang, S.E. Lohse, A.M. Alkilany, L.A. Holland, C. J. Murphy, Nanoparticle–protein interactions: a thermodynamic and kinetic study of the adsorption of bovine serum albumin to gold nanoparticle surfaces, Langmuir 29 (2013) 14984–14996.
[49] E. Blanco, H. Shen, M. Ferrari, Principles of nanoparticle design for overcoming biological barriers to drug delivery, Nat. Biotechnol. 33 (2015) 941–951.
[50] A.B. Chinen, C.M. Guan, C.H. Ko, C.A. Mirkin, The impact of protein corona formation on the macrophage cellular uptake and biodistribution of spherical nucleic acids, Small 13 (2017) 1603847.
[51] S. Abbina, L.E. Takeuchi, P. Anilkumar, K. Yu, J.C. Rogalski, R.A. Shenoi, I. Constantinescu, J.N. Kizhakkedathu, Blood circulation of soft nanomaterials is governed by dynamic remodeling of protein opsonins at nano-biointerface, Nat. Commun. 11 (2020) 3048.
[52] J. Bourquin, A. Milosevic, D. Hauser, R. Lehner, F. Blank, A. Petri-Fink, B. Rothen-Rutishauser, Biodistribution, clearance, and long-term fate of clinically relevant nanomaterials, Adv. Mater. 30 (2018) 1704307.
[53] B. Ouyang, W. Poon, Y.-N. Zhang, Z.P. Lin, B.R. Kingston, A.J. Tavares, Y. Zhang, J. Chen, M.S. Valic, A.M. Syed, P. MacMillan, J. Couture-Senécal, G. Zheng, W.C. W. Chan, The dose threshold for nanoparticle tumour delivery, Nat. Mater. 19 (2020) 1362–1371.
[54] M.P. Nikitin, I.V. Zelepukin, V.O. Shipunova, I.L. Sokolov, S.M. Deyev, P.I. Nikitin, Enhancement of the blood-circulation time and performance of nanomedicines via the forced clearance of erythrocytes, Nat. Biomed. Eng. 4 (2020) 717–731.
[55] W. Li, S. Tutton, A.T. Vu, L. Pierchala, B.S.Y. Li, J.M. Lewis, P.V. Prasad, R. R. Edelman, First-pass contrast-enhanced magnetic resonance angiography in humans using ferumoxytol, a novel ultrasmall superparamagnetic iron oxide (USPIO)-based blood pool agent, J. Magn. Reson. Imag. 21 (2005) 46–52.
[56] B. Thiesen, A. Jordan, Clinical applications of magnetic nanoparticles for hyperthermia, Int. J. Hyperther. 24 (2008) 467–474.
[57] D.K. Chatterjee, P. Diagaradjane, S. Krishnan, Nanoparticle-mediated hyperthermia in cancer therapy, Ther. Deliv. 2 (2011) 1001–1014.
[58] W. Poon, B.R. Kingston, B. Ouyang, W. Ngo, W.C.W. Chan, A framework for designing delivery systems, Nat. Nanotechnol. 15 (2020) 819–829.
[59] S.M. Dadfar, K. Roemhild, N.I. Drude, S. von Stillfried, R. Knüchel, F. Kiessling, T. Lammers, Iron oxide nanoparticles: diagnostic, therapeutic and theranostic applications, Adv. Drug Deliv. Rev. 138 (2019) 302–325.
[60] F. Soetaert, P. Korangath, D. Serantes, S. Fiering, R. Ivkov, Cancer therapy with iron oxide nanoparticles: agents of thermal and immune therapies, Adv. Drug Deliv. Rev. 163 (2020) 65–83.